



Research article

Finite element method analysis of bone stress for variants of locking plate placement

Marek Palka^a, Patrycja Miszczyk^b, Maciej Jurewicz^c, Rafal Perz^{a,*}^a Institute of Aeronautics and Applied Mechanics, Warsaw University of Technology, Nowowiejska 24, 00-660, Warsaw, Poland^b Faculty of Medicine, Medical University of Warsaw, Żwirki i Wigury 61, 02-091, Warsaw, Poland^c Faculty of Applied Informatics and Mathematics, Warsaw University of Life Sciences, Nowoursynowska 159, 02-776, Warsaw, Poland

ARTICLE INFO

Keywords:

Finite element method
Locking plate
Long bone fracture
Stabilization

ABSTRACT

This study investigates the optimal placement of locking plate screws for bone fracture stabilization in the humerus, a crucial factor for enhancing healing outcomes and patient comfort. Utilizing Finite Element Method (FEM) modeling, the research aimed to determine the most effective screw configuration for achieving optimal stress distribution in the humerus bone. A computer tomography (CT) scan of the humerus was performed, and the resulting images were used to create a detailed model in SOLIDWORKS 2012. This model was then analyzed using ANSYS Workbench V13 to develop a finite element model of the bone. Four different screw configurations were examined: $4 \times 0^\circ$, $4 \times 10^\circ$, $4 \times 20^\circ$, $2 \times 20^\circ$; $2 \times 0^\circ$. These configurations were subjected to bending in the XZ and YZ planes, as well as tension and compression along the Z axis. The research identified the $2 \times 20^\circ + 2 \times 0^\circ$ configuration as the most beneficial, with average stress values below 30 MPa and peak stress values below 50 MPa in 3-point bending at the first screw. This configuration consistently showed the lowest stress values across all loading scenarios. Specifically, stress levels ranged from 20 MPa to 50 MPa for bending in the XZ plane, 20 MPa–35 MPa for bending in the YZ plane, 20 MPa–30 MPa for extension in the Z-axis, and 18 MPa–25 MPa for compression in the Z-axis. The $4 \times 10^\circ$ and $4 \times 20^\circ$ configurations also produced satisfactory results, with stress levels not exceeding 70 MPa. However, the $4 \times 0^\circ$ configuration presented considerable stress during bending and compression in the Z-axis, with stress values exceeding 100 MPa, potentially leading to mechanical damage. In conclusion, the $2 \times 20^\circ$; $2 \times 0^\circ$ screw configuration was identified as the most effective in minimizing stress on the treated bone. Future work will involve a more detailed analysis of this methodology and its potential integration into clinical practice, with a focus on enhancing patient outcomes in bone fracture treatment.

1. Introduction

Modern medicine encompasses a wide range of sophisticated methodologies, techniques, and tools that facilitate efficacious diagnosis and treatment of a myriad of injuries and diseases, with an emphasis on treatment planning. The technological evolution of diagnostic apparatus and information systems has rendered the accumulation and examination of multifaceted data pertinent to

* Corresponding author.

E-mail addresses: mpalka@meil.pw.edu.pl (M. Palka), p.a.miszczyn@gmail.com (P. Miszczyk), maciej.jurewicz@sggw.edu.pl (M. Jurewicz), rafal.perz@pw.edu.pl (R. Perz).<https://doi.org/10.1016/j.heliyon.2024.e26840>

Received 17 May 2023; Received in revised form 15 February 2024; Accepted 20 February 2024

Available online 24 February 2024

2405-8440/© 2024 The Authors. Published by Elsevier Ltd. This is an open access article under the CC BY-NC license (<http://creativecommons.org/licenses/by-nc/4.0/>).

individual patients and diseases feasible [1–3]. Such data, gathered during the diagnostic phase, can be leveraged to create virtual models that predict the outcomes of proposed treatments ([4]; Skubich & Piszczatkowski, 2019).

These computational techniques, pivotal in contemporary medicine, hold a significant place in biomechanics, facilitating detailed modeling of distinct human body systems. This manifests in routine activities such as sitting and standing postures [2], ambulation [1, 3], and engaging in specialized activities such as combat sports [5] and acrobatics [6,7]. Additional applications of biomechanics include assessing dental strain [8], constructing microscale models of bones [9], determining bodily center of mass [10], ascertaining bone mineral content relationships [11], and predicting accident outcomes (Jastrzębski & Perz, 2017), among other utilities.

Virtual models lay the groundwork for comprehensive analyses of therapeutic effectiveness, offering the potential to pinpoint the most advantageous solutions for patients. Notably, these models can appraise the effect of skeletal implant geometry [12], delineate the course of patient rehabilitation, such as maneuvering with crutches [13], and assess post-surgical recuperation processes such as knee replacement [14], ligament reconstruction [15,16], or spinal fixation system influences [17].

Within the realm of bone fracture treatment, virtual Computer Aided Design (CAD) modeling and strength analyses such as ANSYS Workbench V13 have shown immense benefits. The selection of appropriate therapy is contingent on multifarious factors including fracture type and location (Ghiasi, 2017), bone properties [18–21], and fixator type [21–24].

Long bone fractures, constituting one of the prevalent forms of skeletal injury [21,22,25], demand careful attention to treatment nuances from stabilizer stiffness to temporal considerations for bone tissue reconstruction [26,27]. Devices such as locking plates exemplify technological integration in bone fusion, allowing for direct intervention at the fracture site [25,27–30].

The interplay of factors such as the stabilization apparatus, fracture type, shape, location, and correct positioning [21,26] exerts a decisive influence on the bone fusion process, underscoring the sophistication and precision incumbent in modern medical practice.

The main aim of the study is to determine the most effective configuration of locking plate screws for bone fracture stabilization in the humerus, focusing on achieving optimal stress distribution to enhance healing outcomes and patient comfort. This objective is pursued to mitigate potential harm to the patient, ensuring a safer and more effective healing process.

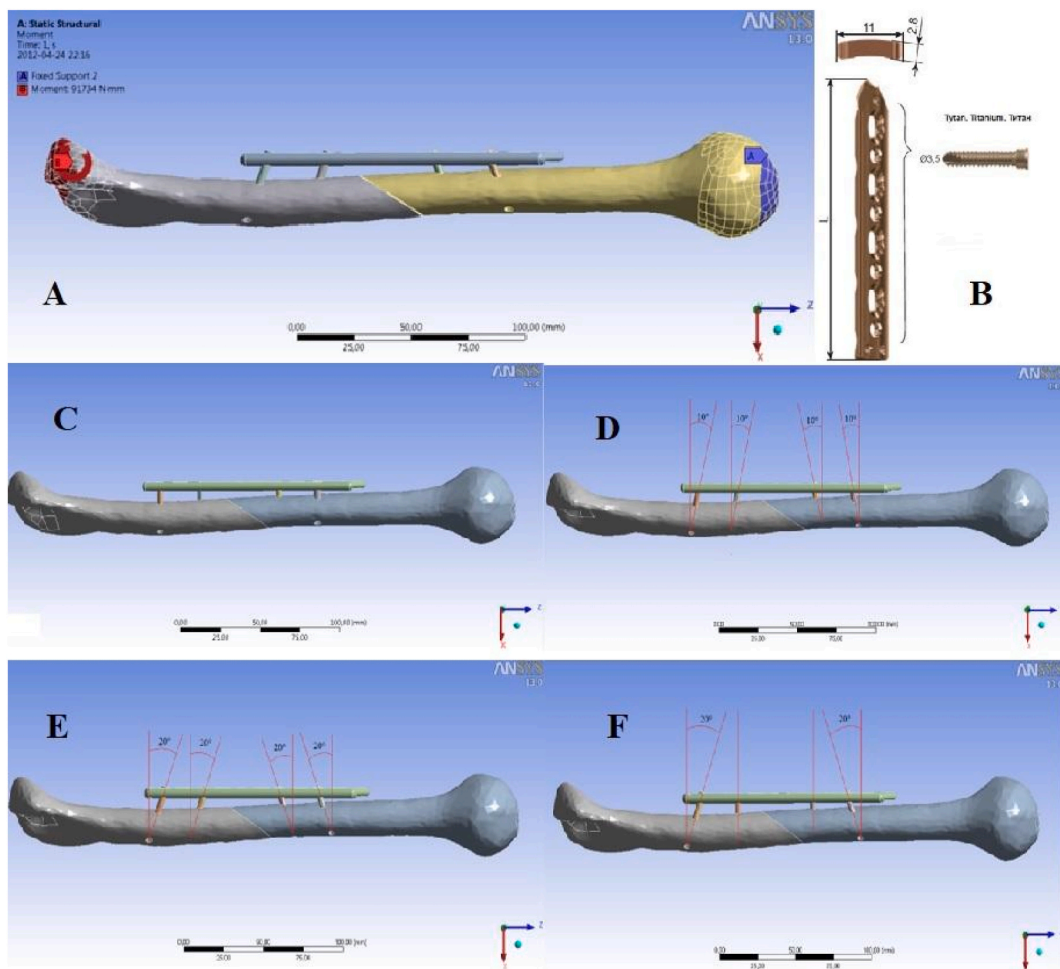


Fig. 1. A) Humerus model used to simulate pulling a stabilizer plate from the bone; B) Geometry of a fixator, $L = 133$ mm; C) Spacing of screws $4 \times 0^\circ$; D) Spacing of screws $4 \times 10^\circ$; E) Spacing of screws $4 \times 20^\circ$; F) Spacing of screws $2 \times 20^\circ$, $2 \times 0^\circ$.

The analysis involved examination of the stresses, displacements and static deformations present in the screws and fixator secured in the humerus under a number of screw placement configurations. The maximum displacements occurring at the fracture site under applied force were calculated. The comprehensive picture of the stresses present in the fixator plate, screws and bone was possible through the capabilities of the ANSYS Workbench V13 environment.

The research problem focused on the bone stabilization and relationship between parameters describing the state and condition of cortical bone tissue. To address this, a material model of cortical bone tissue and a detailed numerical model of humerus, which was then "fractured" in a single location, were created. The two resulting bone pieces were then connected with a locking plate stabilizer. Its elements (plate and screws) were selected from a catalog (ChM sp. z o. o. company catalog). Parametric analysis and calculations were performed using ANSYS Workbench V13 system. The proposed material model considers the physical properties of bone tissue and the metal comprising the fixator's plate and screws. The data pertaining to the material properties of bone tissue were sourced from the literature [31]. The simulation process followed similar methods to those in the literature [32], focusing on potential damage to the bone with the plate stabilizer mounted on it, and examining practical significance of the screw attachment angle to the bone. The simulations assumed the presence of smaller forces that occur during daily function.

2. Materials and methods

The aim of research is to pinpoint the optimal configuration for screw placement configuration in bone fracture stabilization that minimizes stress exerted on the bone.

The cortical bone was modeled as an orthotropic material with the following properties: orthotropic material, $\rho = 1.39 \text{ g/cm}^3$, $E_1 = 3880.6 \text{ MPa}$, $E_2 = 3880.6 \text{ MPa}$, $E_3 = 5712.6 \text{ MPa}$, $G_{12} = 5.71 \text{ MPa}$, $G_{23} = 7.11 \text{ MPa}$, $G_{31} = 6.58 \text{ MPa}$, $\nu_{12} = 0.4$, $\nu_{23} = 0.25$, $\nu_{31} = 0.25$ [33].

The material properties of the locking plate and screws: isotropic material, taken from ANSYS material base: bone density $\rho = 4.62 \text{ g/cm}^3$, elastic modulus for cortical or trabecular bone $E = 96000 \text{ MPa}$, shear modulus $G = 35294 \text{ MPa}$, Poisson ratio $\nu = 0.36$ [31].

Utilizing SOLIDWORKS 2012 software, a computer mathematical model of the fractured bone was created based on CT scans. This model, including the bone and plate stabilizer, was then imported into ANSYS Workbench V13 for further analysis. The model focused solely on the cortical layer of the bone, assuming orthotropic properties. The visco-elastic properties of bone tissue were neglected. An ideal connection between bone and stabilizer elements was assumed, along with a perfect friction model (friction coefficient $\mu = 0$) at contact points. The coordinate system was aligned with the Z axis along the bone, the X axis perpendicular to the stabilizer's main surface, and the Y axis perpendicular to both X and Z axes. The point of force application was assumed to be on the block and the epicondyle with restraint on the head of the bone (Fig. 1A). Gravitational forces were not considered.

The fixator's geometry was designed based on technical documentation. The design consists of screws with threaded heads and a locking plate designed by CHM Sp. z o. o (ChM sp. z o. o. company catalogue) (Fig. 1B).

The process of strain determination in this study was methodically structured and executed in a sequential manner. Initially, the investigation began with the acquisition of CT scans of the bone fracture. These scans provided the detailed anatomical data necessary for the subsequent modeling phase. Following the data collection, the next step involved the development of a precise bone model. This task was accomplished using SOLIDWORKS 2012 software, which allowed for an accurate representation of the bone's geometry and structure. The model included not only the bone but also the plate stabilizer, ensuring a comprehensive representation of the fracture stabilization system.

Once the bone model was complete, it was imported into ANSYS Workbench V13 for further analysis. This transition marked a shift from design to simulation, enabling the application of various mechanical scenarios to the model. In ANSYS Workbench, the points of contact were meticulously designed. These included the interfaces between the fixator and screws, the screws and the bone, and between the left and right bone fragments. Such detailed modeling was crucial for accurately simulating the mechanical interactions within the stabilization system.

The next phase involved building a mesh of the model. This was achieved using the Hex dominant method, which utilized hexagonal elements for the bone and screws, and triangular elements (Tetrahedron) for the fixator's plate. The mesh comprised approximately 16,500 elements, with a 2 mm element size for the bone and screws, ensuring a high level of detail in the simulation.

Subsequently, the model was subjected to various mechanical tests, including bending, extension, and compression. During these tests, appropriate forces, moments, and fixator positions were applied to the bone model. This step was critical in evaluating the performance of the stabilization system under different loading conditions. The analysis of strains in the bone tissue was then conducted for each test scenario. This involved assessing the numerical values of the maximum stresses occurring near the screw for each case. By comparing these results, the most favorable screw configuration was determined, which exhibited the lowest stresses and, consequently, the least amount of potential bone damage.

Finally, the study also included an analysis of displacements in the area of the fracture. This was performed using the "Sliding Distance" function in ANSYS, which represents the sum of the path along the movement. The displacement was not only graphically presented but also quantitatively measured, with the maximum value being calculated. This function was instrumental in detecting where bone fragments overlap and determining their relative displacement, providing valuable insights into the mechanical stability of the fracture under various conditions.

During the analysis, the screws configurations: $4 \times 0^\circ$ (Figs. 1C), $4 \times 10^\circ$ (Figs. 1D), $4 \times 20^\circ$ (Figs. 1E) and $2 \times 20^\circ + 2 \times 0^\circ$ (Fig. 1F) were examined for bending (both XZ and YZ planes), compression and tension. The $4 \times 0^\circ$ (Figs. 1C), $4 \times 10^\circ$ (Figs. 1D), and $4 \times 20^\circ$ (Fig. 1E) screw placement configurations were selected based on literature [32], where $2 \times 0^\circ$, $2 \times 10^\circ$, and $2 \times 20^\circ$ was chosen to test a mixed screw arrangement.

In Case No. 1, the following boundary conditions were assumed (Fig. 2).

- A fixed support was applied to the head of the bone;
- A bending moment was applied to the distal end of the bone in the XZ plane.

This case can be interpreted as normal movement of the arm in the shoulder, perpendicular to a body position.

During the simulation, stress distribution was acquired for each screw hole in the bone. A moment of force $M = 15000$ Nmm (50 N force applied on a lever arm of 300 mm) was applied for each screw fixation configuration in the bone.

In Case No. 2, the following boundary conditions were assumed (Fig. 4).

- A fixed support was applied to the head of the bone;
- A bending moment was applied to the distal end of the bone in the YZ plane.

During the simulation a stress distribution was obtained for each screw hole in the bone. A moment of force $M = 10000$ Nmm was applied for each screw fixation configuration in the bone.

This case can be interpreted as normal movement of the arm in the shoulder, parallel to a body position.

In Case No. 3, the following boundary conditions were assumed (Fig. 6).

- A fixed support was applied to the head of the bone;
- An extending force was applied to the distal end of the bone along the Z-axis.

This case can be interpreted as a static load inserted on the arm bone when carrying a heavy object.

During the simulation, a stress distribution in each screw hole in the bone was acquired. A force $F = 500$ N was applied to each screw fixation configuration in the bone.

In Case No. 4, the following boundary conditions were assumed (Fig. 8).

- A fixed support was applied to the head of the bone;
- A compressing force was applied to the distal end of the bone along the Z-axis.

This case can be interpreted as load exerted on the bone due to actions like pushing or pressing, or bearing the weight of the body.

During the simulation, a stress distribution was acquired in each screw hole in the bone. A force $F = 500$ N was applied for each configuration of screws fixation in the bone.

3. Results

3.1. Case no. 1 – bending in the XZ plane

In the $4 \times 0^\circ$ configuration (Fig. 3A), analysis of the model revealed displacements ranging from 0 to 1.1599 mm. In this case, an area of sliding was observed around the fracture location on the distal bone fragment. In the $4 \times 10^\circ$ configuration (Fig. 3B), displacement values ranged from 0 to a maximum of 0.8714 mm for this configuration. Increasing the angle at which the screw was fastened in the bone resulted in an irregular sliding pattern. In the $4 \times 20^\circ$ configuration (Fig. 3C), the displacement values ranged from 0 to a maximum of 1.087 mm for this configuration. A significant reduction in the slip area near the fracture edge was observed. In the $2 \times 20^\circ$ and $2 \times 0^\circ$ configurations (Fig. 3D), displacement values ranged from 0 and the maximum 1.1216 mm for this configuration. The displacement no longer concentrates in the central part of the “fracture”, like in the other cases, but occurred on its edges. This indicates that the location of the fracture has the least risk of displacement, leading to improved stability and faster patient recovery.

The maximum equivalent stresses values in each hole indicate that the larger screw fixation angles result in increased stress in the bone tissue. In cases of bone bending, a $2 \times 20^\circ$, $2 \times 0^\circ$ screw configuration should be utilized. This configuration reduces the stress

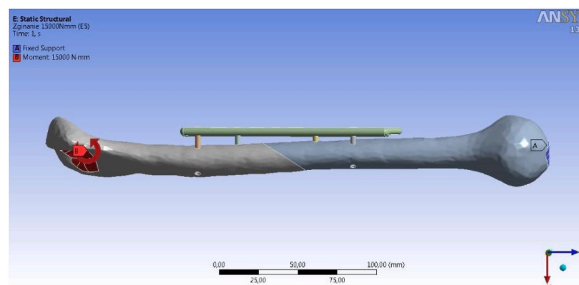


Fig. 2. Boundary conditions of case No. 1 - bending in the XZ plane.

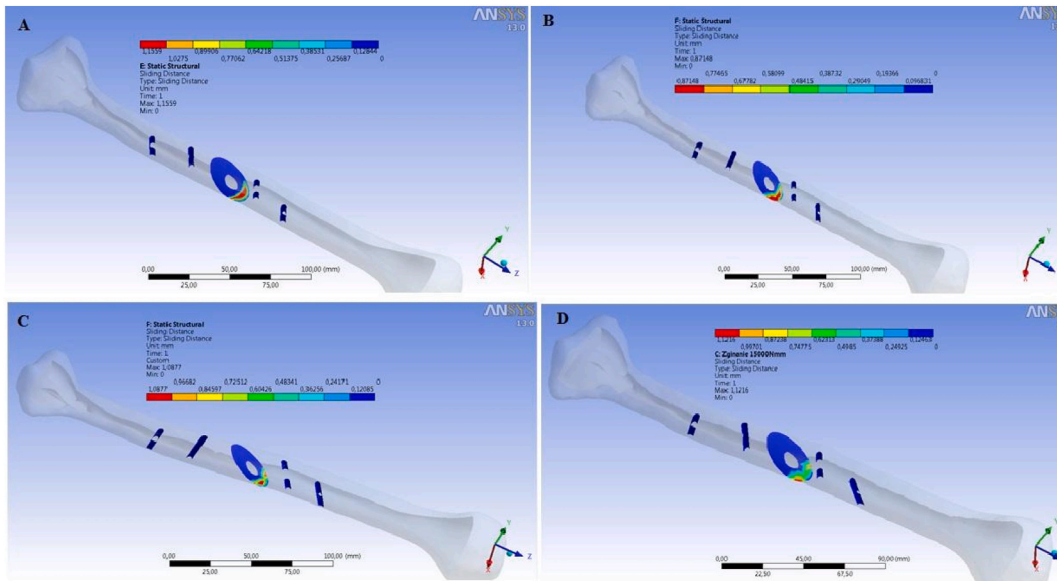


Fig. 3. The sliding that appeared in the location of contact between two bone fragments of case No. 1: A) $4 \times 0^\circ$, B) $4 \times 10^\circ$, C) $4 \times 20^\circ$, D) $2 \times 20^\circ$, $2 \times 0^\circ$.

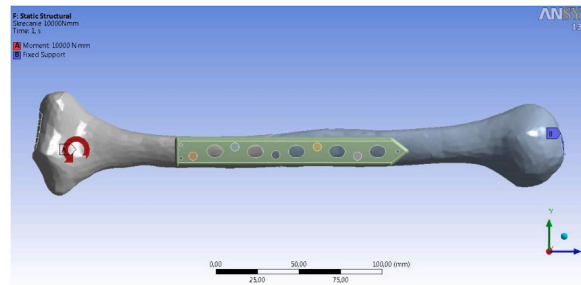


Fig. 4. Boundary conditions of case No. 2 - bending in the YZ plane.

appearing in the screw trajectory and decreases the displacement area near the fracture location, which can significantly expedite bone healing.

3.2. Case no. 2 – bending in the YZ plane

In the $4 \times 0^\circ$ configuration (Fig. 5A), there were almost no stresses near the fracture, resulting in minimal displacement. The largest displacement was 0.4633 mm marked in red. In the $4 \times 10^\circ$ configuration (Fig. 5B), the maximum displacement was slightly higher at 0.46395 mm, similarly to the previous case. The displacement area, as can be seen in the image above, increased. In the $4 \times 20^\circ$ configuration (Fig. 5C), the maximum displacement, marked in red, was 0.5605 mm. This is a relatively small displacement, but its value is almost 20% higher compared to the previous configuration. In the $2 \times 20^\circ$, $2 \times 0^\circ$ configuration (Fig. 5D), the maximum displacement was 0.402 mm, the smallest of all the configurations. However, this configuration resulted in the least stable fracture. Although the sliding distance was the smallest, the reduced stability of the fracture site compared to the other cases must be considered.

The maximum equivalent stress values in each hole indicate that larger screw fixation angles result in increased stresses in the bone tissue. In cases of lateral bending of the bone, a $2 \times 20^\circ$, $2 \times 0^\circ$ screw configuration should be used. This configuration reduces the stress in the screw paths. Despite the fact that the displacement area of the fracture location is the largest, this configuration should still be considered, because the stresses in the screw paths should be the smallest. As a result, the risk of bone damage can be minimized.

3.3. Case no. 3 – extension in the Z-axis

In the $4 \times 0^\circ$ configuration (Fig. 7A), the sliding area is small and the maximum displacement of bone fragments is 0.3237 mm. The warmer the color on the scale, the more one half of the stabilized bone overlaps the other. In the $4 \times 10^\circ$ configuration (Fig. 7B), the

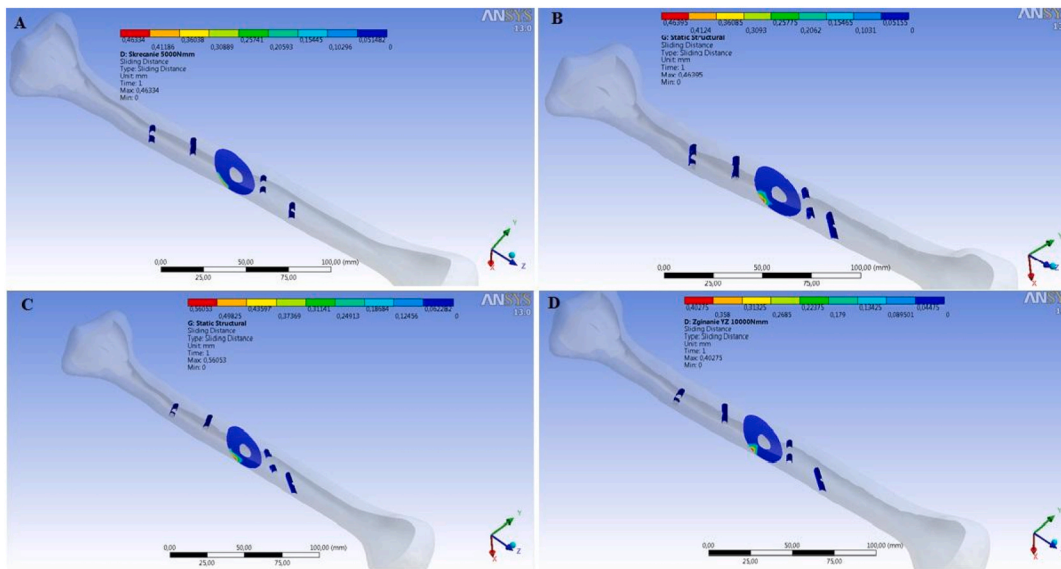


Fig. 5. The sliding that appeared in the location of contact between two bone fragments of case No. 2: A) $4 \times 0^\circ$, B) $4 \times 10^\circ$, C) $4 \times 20^\circ$, D) $2 \times 20^\circ, 2 \times 0^\circ$.

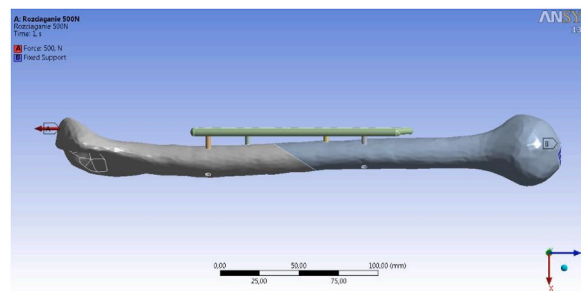


Fig. 6. Boundary conditions of case No. 3 - extension in the Z-axis.

displacement values are comparable to those from the previous configuration – they are at most 5% lower and stand at 0.3077 mm. In the $4 \times 20^\circ$ configuration (Fig. 7C), the maximum displacement is 0.3224 mm the same as in the $4 \times 0^\circ$ case. In the $2 \times 20^\circ, 2 \times 0^\circ$ configuration (Fig. 7D), the area of displacements occurring during sliding is noticeably larger, but the maximum displacement value is 0.1594 mm, which means it's over 100% lower than in the previous configurations. Considering both the stresses occurring in the holes and the stability of the fracture site, this case provides the optimal solution for bone extension in the Z-axis.

The maximum equivalent stress values in each hole indicate that larger screw fixation angles cause more stresses in the bone tissue. When an extending force is applied to a patient's bone, a $2 \times 20^\circ, 2 \times 0^\circ$ screw configuration should be used. This will reduce stress formation in the screw paths.

3.4. Case no. 4 – compression in the Z-axis

In the $4 \times 0^\circ$ configuration (Fig. 9A), the maximum displacement that occurred during sliding is marked in red. This displacement can be found in the upper part of the fracture measuring 0.7554 mm. Additionally, sliding also occurs in the right region of the fracture. In the $4 \times 10^\circ$ configuration (Fig. 9B), the maximum displacements occurring in the bone are marked in red and measure at 0.4764 mm. In the $4 \times 20^\circ$ configuration (Fig. 9C), the area of sliding is comparable to the $4 \times 0^\circ$ configuration, but the maximum displacement value decreased by over 360%, measuring at 0.1646 mm. This displacement is so marginal that the stability of the fracture site during compression in this configuration can be considered ideal. For $2 \times 20^\circ, 2 \times 0^\circ$ configuration (Fig. 9D), the maximum stresses occur in three different areas of the lower parts of the fracture, as highlighted in red in the image above. The maximum stresses have increased to about 0.718 mm, indicating poorer stability compared to the previous cases.

The maximum equivalent stress values in each hole indicate that larger angles of screw fixation cause greater stress in the bone tissue. When a patient's bone is exposed to compression, a $2 \times 20^\circ, 2 \times 0^\circ$ configuration should be used. This leads to a reduction in the stresses occurring along the screw paths.

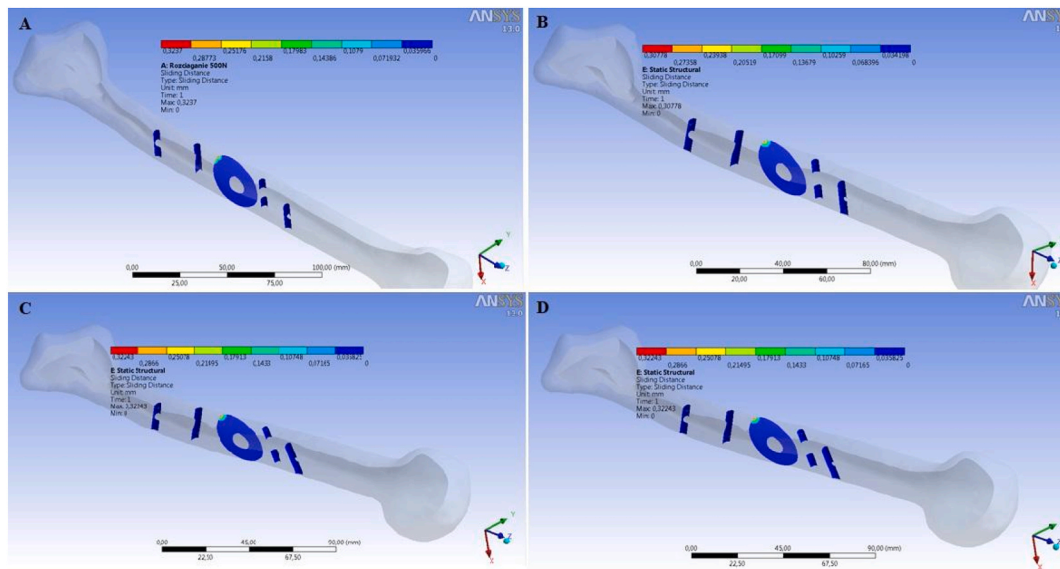


Fig. 7. The sliding that appeared in the location of contact between two bone fragments of case No. 3: A) $4 \times 0^\circ$, B) $4 \times 10^\circ$, C) $4 \times 20^\circ$, D) $2 \times 20^\circ$, $2 \times 0^\circ$.

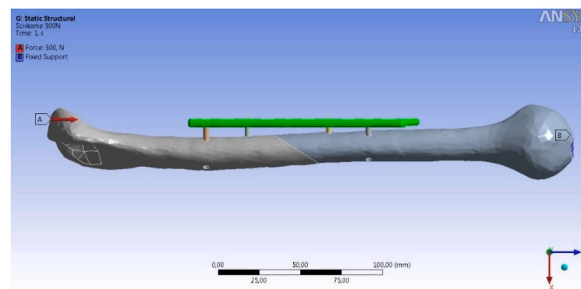


Fig. 8. Boundary conditions of case No. 4 - compression in the Z-axis.

3.5. Summary

The purpose of this research was to identify the optimal configuration of stabilizing screws in the humerus that minimizes stress on the patient's bone. The screw configurations evaluated were $4 \times 0^\circ$, $4 \times 10^\circ$, $4 \times 20^\circ$ and $2 \times 20^\circ$; $2 \times 0^\circ$. To perform the numerical analysis in ANSYS Workbench V13, a model based on CT scans of the fractured bone was developed in the SOLIDWORKS 2012 environment. Simulation results showed that the best placement of the screws within the humerus was a $2 \times 20^\circ + 2 \times 0^\circ$ configuration. In this setup, the stress levels were the lowest, averaging under 30 MPa and peaking at no more than 50 MPa. While the $4 \times 0^\circ$, $4 \times 10^\circ$ and $4 \times 20^\circ$ configurations yielded satisfactory outcomes, however, they did register higher stresses than the $2 \times 20^\circ$; $2 \times 0^\circ$ configurations. Notably, the stress results for the $4 \times 0^\circ$, $4 \times 10^\circ$ and $4 \times 20^\circ$ configurations did not exceed 70 MPa, which is still significantly under the bone's strength threshold of 100 MPa.

Simulations of the stresses during bending in the XZ plane showed stress levels ranging from 20 MPa to 50 MPa for $2 \times 20^\circ$, $2 \times 0^\circ$ configuration (Fig. 10A). Similarly, bending simulation for the same configurations in the YZ plane indicated that stress levels between 20 MPa and 35 MPa (Fig. 10B). Extension simulation in the Z-axis for these configurations indicated the displayed stress levels from 20 MPa to 30 MPa (Fig. 10C), and Z-axis compression simulation resulted in stress levels ranging from 18 MPa to 25 MPa (Fig. 10D).

4. Discussion

The aim of this study was to analyze the optimal configuration of the locking plate screw arrangement in the bone to minimize stress, thus reducing potential harm to patient health. Stress levels, displacements and static deformations in the screws and stabilizer fastened within the forearm bone were analyzed. The research identified the most beneficial configuration to be $2 \times 20^\circ + 2 \times 0^\circ$. This setup generated averaged stress values below 30 MPa and peaks stress values below 50 MPa (3 point bending, 1st screw). Among all

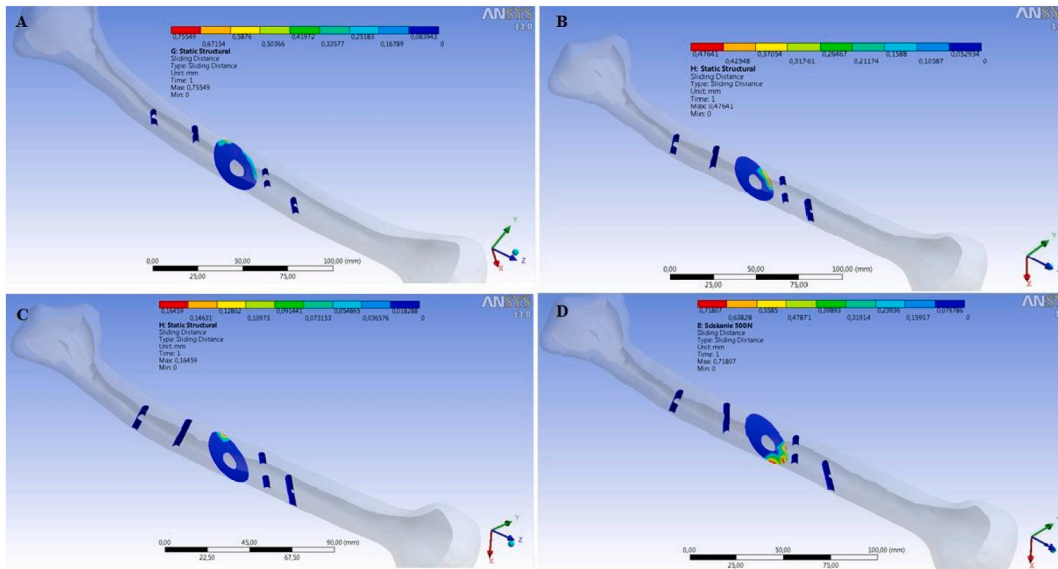


Fig. 9. The sliding that appeared in the location of contact between two bone fragments of case No. 4: A) $4 \times 0^\circ$, B) $4 \times 10^\circ$, C) $4 \times 20^\circ$, D) $2 \times 20^\circ$, $2 \times 0^\circ$.

configurations analyzed, this yielded the lowest stress values. Other configurations provided satisfactory results but showed slightly higher stress levels. However, all of the stress results remained below 70 MPa, significantly below the estimated bone endurance threshold of 100 MPa.

Simulations were carried out for four different load scenarios on bones fixed with varying screw configurations. The resulting stress values are presented in the graphs below. The optimal screw configuration in the bone $2 \times 20^\circ$, $2 \times 0^\circ$, is highlighted in green (Fig. 10A–B, Fig. 10C–D). This configuration resulted in the lowest occurring stress levels. Both $4 \times 10^\circ$ and $4 \times 20^\circ$ configurations led to stress levels not exceeding 70 MPa, which falls within the safe range for the skeletal system, given that the endurance limit of bone tissue is set at 100 MPa. Consequently, $4 \times 10^\circ$ and $4 \times 20^\circ$ configurations can be successfully employed for bone-fixator conjunctions.

The $4 \times 0^\circ$ configuration, however, yielded considerable stress during bending (around 80 MPa) and compression in the Z-axis. When the load compressed the bone along the Z-axis, stress values exceeded 100 MPa, the rough estimate of bone endurance limit. This could directly contribute to mechanical damage in two of the holes, making the $4 \times 0^\circ$ configuration inadvisable for compressive loads. Given that a patient's bone is subjected to complex loads (a combination of analyzed cases) it is recommended to avoid using the $4 \times 0^\circ$ configuration.

This study provides insights into the potential use of FEM as a tool for pre-surgery planning. While the study uses a simplified model of screw connections, more advanced models of multi-screwed connections can also be applied as presented in Ref. [34,35]. FEM could be further used to analyze maximum stress, stress distribution and displacement of the fixation and nonunion site under increasing axial and torsional load [36]. FEM analysis facilitates the selection of appropriate screw material, determination of the optimum number of screws in the stabilizer and their correct positioning ([37]; Kaisidis, et al., 2018 [38,39]; [40–47]).

The impact of screw placement configurations was determined both through simulation and experimental methods. The experiment described in Ref. [32] showed that aligning screws parallel to the bone (0°) reduces bone damage by 47%, compared to a 20° configuration. The results from a model created for the purpose of this work closely mirrored experimental findings, affirming the validity of the assumptions and model design. Noted discrepancies may result from different fixator designs research materials (bovine/humane bone).

In [48], the optimal design of internal fixation parameters was explored to maximize the stability and healing efficiency of the plate fixation system. The results suggest that optimal screw configuration can significantly enhance the biomechanical environment, promoting the bone healing process.

Stress analysis for various loading cases, such as bending in the XZ and YZ planes, Z-axis tension and Z-axis compression, demonstrated that the $2 \times 20^\circ + 2 \times 0^\circ$ configuration consistently resulted in the lowest bone stresses across all examined cases. When compared with experimental studies found in the literature [32] these simulation results align well with the data obtained from real-world situations. The optimal $2 \times 20^\circ + 2 \times 0^\circ$ configuration minimizes bone damage, potentially accelerating patient's healing process and enhancing their comfort during treatment.

5. Conclusions

This study's primary achievement lies in the identification of the optimal screw configuration for stabilizing fractures in the humerus, a critical aspect in orthopedic surgery aimed at minimizing stress on the bone. The research meticulously analyzed various

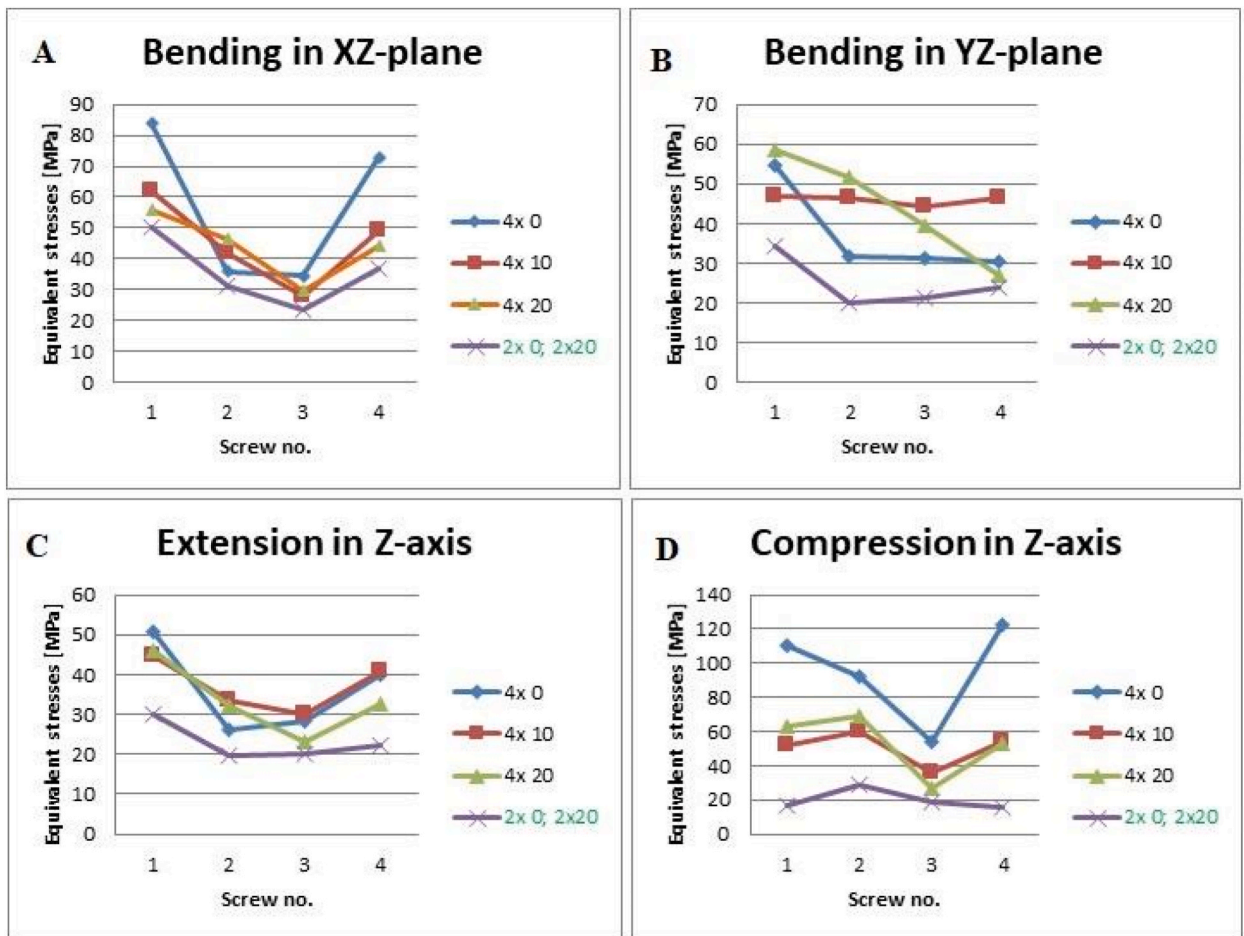


Fig. 10. Stress values for screw arrangement configurations: A – Bending in XZ-plane, B – Bending in YZ-plane, C – Extension in Z-axis, D – Compression in Z-axis.

screw configurations using FEM simulations, a process that has proven invaluable in surgical planning and decision-making. The major success of this study is the identification of the $2 \times 20^\circ + 2 \times 0^\circ$ screw configuration as the optimal arrangement for stabilizing humerus fractures, effectively minimizing stress on the bone. This configuration demonstrated superior performance, with stress levels averaging below 30 MPa and peaking at no more than 50 MPa, significantly lower than other tested configurations ($4 \times 0^\circ$, $4 \times 10^\circ$, and $4 \times 20^\circ$). The $2 \times 20^\circ + 2 \times 0^\circ$ arrangement not only ensures lower stress levels but also enhances stability during the bone healing process, marking a significant advancement in orthopedic surgical planning for fracture treatment. This finding is pivotal in guiding the selection of screw configurations for bone stabilization, directly impacting the effectiveness of healing and reducing the risk of stress-related complications.

The $2 \times 20^\circ + 2 \times 0^\circ$ arrangement not only ensures lower stress levels but also contributes to enhanced stability during the bone healing process. This finding marks a significant advancement in the field of orthopedic surgical planning for fracture treatment. By adopting this screw configuration, surgeons can potentially improve healing outcomes and reduce the likelihood of complications associated with stress-induced damage during the healing process. The study's results underscore the effectiveness of the $2 \times 20^\circ + 2 \times 0^\circ$ configuration in enhancing bone stabilization, thereby providing a valuable tool for orthopedic surgeons in their clinical practice. Furthermore, the findings from this research have broader implications beyond the immediate scope of humerus fracture treatment. They serve as a foundation for further research and analysis of more intricate models of multi-screw joints and the application of various materials in orthopedic surgery. The insights gained from this study can guide future investigations into the biomechanics of bone stabilization, contributing to the development of more effective surgical techniques and materials.

In conclusion, this research highlights the critical role of selecting the right screw configuration for bone stabilization in significantly impacting stress minimization and damage reduction during the healing process. The recommended $2 \times 20^\circ + 2 \times 0^\circ$ configuration provides a scientifically backed solution that enhances stability and minimizes stress on the bone, thereby improving patient outcomes in the treatment of fractures and other bone conditions. This study not only contributes valuable knowledge to the field of orthopedic surgery but also paves the way for future advancements in surgical techniques and materials.

Data availability statement

Presented data has not been deposited into a publicly available repository. The used data is confidential.

CRediT authorship contribution statement

Marek Palka: Software, Project administration, Methodology, Investigation, Formal analysis, Data curation, Conceptualization. **Patrycja Miszczyk:** Writing – original draft, Software, Resources, Methodology, Investigation. **Maciej Jurewicz:** Writing – original draft, Validation, Methodology, Investigation, Formal analysis, Data curation. **Rafal Perz:** Writing – review & editing, Writing – original draft, Supervision, Project administration, Methodology, Conceptualization.

Declaration of competing interest

The authors declare that they have no known competing financial interests or personal relationships that could have appeared to influence the work reported in this paper.

References

- [1] J. Pauk, Computerized analysis and modelling of patients with deformities of lower limbs, *Acta Bioeng. Biomech.* 11 (1) (2009) 47–51.
- [2] K. Nowakowska, M. Gzik, R. Michnik, A. Myśliwiec, J. Jurkojc, S. Suchoń, M. Burkacki, The loads acting on lumbar spine during sitting down and standing up, *Innovations in Biomedical Engineering. Advances in Intelligent Systems and Computing* 526 (2017) 169–176, https://doi.org/10.1007/978-3-319-47154-9_20. Springer: Cham, Germany.
- [3] K. Arkusz, T. Klekiel, T.M. Niezgodna, R. Będziński, The influence of osteoporotic bone structures of the pelvic-hip complex on stress distribution under impact load, *Acta Bioeng. Biomech.* 20 (1) (2018) 29–38, <https://doi.org/10.5277/ABB-00882-2017-02>.
- [4] M. Błażkiewicz, A. Wit, Artificial neural network simulation of lower limb joint angles in normal and impaired human gait, *Acta Bioeng. Biomech.* 20 (3) (2018) 43–49, <https://doi.org/10.5277/ABB-01129-2018-02>.
- [5] K. Buško, P.T. Nikolaidis, Biomechanical characteristics of Taekwondo athletes: kicks and punches vs. laboratory tests, *Biomed. Hum. Kinet.* 10 (1) (2018) 81–88, <https://doi.org/10.1515/bhk-2018-0013>.
- [6] A. Czaplicki, K. Dziewiecki, T. Sacewicz, Identification of internal loads at the selected joints and validation of a biomechanical model during performance of the handspring front somersault, *Acta Mech. Automatica* 6 (2) (2012) 28–32.
- [7] K. Dziewiecki, W. Blajer, Z. Mazur, A. Czaplicki, Modeling and computational issues in the inverse dynamics simulation of triple jump, *Multibody Syst. Dyn.* 32 (3) (2014) 299–316, <https://doi.org/10.1007/s11044-013-9375-6>.
- [8] G. Milewski, Numerical and experimental analysis of effort of human tooth hard tissues in terms of proper occlusal loadings, *Acta Bioeng. Biomech.* 7 (1) (2005) 47–59.
- [9] M. Pawlikowski, K. Jankowski, K. Skalski, New microscale constitutive model of human trabecular bone based on depth sensing indentation technique, *J. Mech. Behav. Biomed. Mater.* 85 (2018) 162–169, <https://doi.org/10.1016/j.jmbm.2018.05.036>.
- [10] W.S. Erdmann, R. Kowalczyk, A personalized method for estimating centre of mass location of the whole body based on differentiation of tissues of a multi-divided trunk, *J. Biomech.* 48 (1) (2015) 65–72, <https://doi.org/10.1016/j.jbiomech.2014.11.001>.
- [11] A. Mazurkiewicz, T. Topoliński, Relationship between the mineral content of human trabecular bone and selected parameters determined from fatigue test at stepwise-increasing amplitude, *Acta Bioeng. Biomech.* 19 (3) (2017) 19–26, <https://doi.org/10.5277/ABB-00722-2016-02>.
- [12] P. Prochor, E. Sajewicz, The influence of geometry of implants for direct skeletal attachment of limb prosthesis on rehabilitation program and stress-shielding intensity, *BioMed Res. Int.* (2019) 6067952, <https://doi.org/10.1155/2019/6067952>.
- [13] A. Rzepnicka, J. Kabaciński, M. Murawa, A. Fryzowicz, M. Syczewska, B.L. Dworak, Biomechanical evaluation of swing-through crutch gait in patients with lower extremity injury, *Acta Bioeng. Biomech.* 22 (1) (2020) 111–117, <https://doi.org/10.37190/ABB-01455-2019-03>.
- [14] A. Hadamus, D. Białoszewski, M. Błażkiewicz, A.J. Kowalska, E. Urbaniak, K.T. Wydra, K. Wiaderna, R. Boratynski, A. Kobza, W. Marczyński, Assessment of the effectiveness of rehabilitation after total knee replacement surgery using sample entropy and classical measures of body balance, *Entropy* 23 (2) (2021) 164, <https://doi.org/10.3390/e23020164>.
- [15] S. Winiarski, A. Czamara, Evaluation of gait kinematics and symmetry during the first two stages of physiotherapy after anterior cruciate ligament reconstruction, *Acta Bioeng. Biomech.* 14 (2) (2012) 91–100, <https://doi.org/10.5277/abb120212>.
- [16] A. Czaplicki, W. Kuniszkyk-Józkowiak, J. Jaszczuk, M. Jarocka, J. Walawski, Using the discrete wavelet transform in assessing the effectiveness of rehabilitation in patients after ACL reconstruction, *Acta Bioeng. Biomech.* 19 (3) (2017) 139–146, <https://doi.org/10.5277/ABB-00749-2016-02>.
- [17] K. Szkoda, C. Pezowicz, Finite element analysis of fixation system influence on the thoracolumbar spine stability, *Appl. Mech. Mater.* 821 (2016) 685–692, <https://doi.org/10.4028/www.scientific.net/amm.821.685>.
- [18] A. Nikodem, K. Ścigała, Impact of some external factors on the values of mechanical parameters determined in tests on bone tissue, *Acta Bioeng. Biomech.* 12 (3) (2010) 85–93.
- [19] A. Nikodem, Correlations between structural and mechanical properties of human trabecular femur bone, *Acta Bioeng. Biomech.* 14 (2) (2012) 37–46, <https://doi.org/10.5277/abb120205>.
- [20] F.A. Sabet, A.R. Najafi, E. Hamed, I. Jasiuk, Modelling of bone fracture and strength at different length scales: a review, *Interface Focus* 6 (1) (2016) 20150055, <https://doi.org/10.1098/rsfs.2015.0055>.
- [21] L.P. Chee, R.B. Daud, S.F.K. Mohamad Khan, N.A. Md Zain, Y. Bajuri, Pre-drilling and self-drilling pins screw-bone fixation stress interaction analysis induced by uniaxial compression loading, *Malays. J. Fundam. Appl. Sci.* 15 (1) (2019) 99–108, <https://doi.org/10.11113/mjfas.v15n2019.1006>.
- [22] J.C. Laux, F. Grubhofer, C.M.L. Werner, H. Simmen, G. Osterhoff, Current concepts in locking plate fixation of proximal humerus fractures, *J. Orthop. Surg. Res.* 12 (2017) 137, <https://doi.org/10.1186/s13018-017-0639-3>.
- [23] H. Matsubara, H. Tsuchiya, Treatment of bone tumor using external fixator, *J. Orthop. Sci.* 24 (1) (2019) 1–8, <https://doi.org/10.1016/j.jos.2018.06.022>.
- [24] A.M. Amaro, M.F. Paulino, L.M. Roserio, M.A. Neto, The effect of external fixator configurations on the dynamic compression load: an experimental and numerical study, *Appl. Sci.* 10 (1) (2020) 3, <https://doi.org/10.3390/app10010003>.
- [25] J. Li, X. Zhao, X. Hu, C. Tao, R. Ji, A theoretical analysis and finite element simulation of fixator–bone system stiffness on healing progression, *J. Appl. Biomater. Funct. Mater.* 16 (3) (2018) 115–125, <https://doi.org/10.1177/2280800017750357>.
- [26] N.A. Zainudin, M.H. Ramlie, H.F.M. Latip, A. Azaman, G.H. Seng, E. Garcia-Nieto, M.R.A. Kadir, Biomechanical evaluation of pin placement of external fixator in treating transverse tibia fracture: analysis on first and second cortex of cortical bone, *Malays. J. Fundam. Appl. Sci.* 15 (1) (2019) 75–79, <https://doi.org/10.11113/mjfas.v15n2019.1263>.
- [27] X. Zhao, J. Li, X. Hu, C. Tao, R. Ji, Investigation of load transfer process between external fixator and bone model by experimental and finite element methods, *J. Appl. Biomater. Funct. Mater.* 17 (1) (2019) 1–11, <https://doi.org/10.1177/2280800019826512>.
- [28] R. Będziński, *Biomechanika Inżynierska, Zagadnienia Wybrane, Oficyna Wydawnicza Politechniki Wrocławskiej: Wrocław, Poland, 1997.*

- [29] A. MacLeod, A.H.R.W. Simpson, P. Pankaj, Experimental and numerical investigation into the influence of loading conditions in biomechanical testing of locking plate fracture fixation devices, *Bone Jt. Res.* 7 (1) (2018) 111–120, <https://doi.org/10.1302/2046-3758.71.BJR-2017-0074.R2>.
- [30] X. Shi, H. Liu, W. Mei, L. Zhang, L. Ding, Z. Huang, P. Wang, Effect of intramedullary nail and locking plate in the treatment of proximal humerus fracture: an update systematic review and meta-analysis, *J. Orthop. Surg. Res.* 14 (2019) 285, <https://doi.org/10.1186/s13018-019-1345-0>.
- [31] E.M.M. Fonesca, M.J. Lima, L.M.S. Barreira, Human femur assessment using isotropic and orthotropic materials dependent of bone density, in: *Proceedings of the 3rd International Conference on Integrity, Reliability and Failure*, Porto, Portugal, July 2009, pp. 20–24.
- [32] D. Wähnert, M. Windolf, S. Brianza, S. Rothstock, R. Radtke, V. Brighenti, K. Schwieger, A comparison of parallel and diverging screw angles in the stability of locked plate constructs, *Bone Jt. J.* 93-B (9) (2011) 1259–1264, <https://doi.org/10.1302/0301-620X.93B9.26721>.
- [33] R.J. Beer, J. Eberhardsteiner, J. Kodvanj, W. Grienauer, F. Gottsauner-Wolf, G. Skrbensky, Mechanical and medical aspects of an implant-bone connection in the femur: a three-dimensional photoelastic study of the load transfer mechanism using gamma radiation for fixing the experimental information. Comparison of two solutions of femur prosthesis, *Acta Bioeng. Biomech.* 2 (2) (2000) 25–31.
- [34] R. Grzejda, Modelling nonlinear preloaded multi-bolted systems on the operational state, *Eng. Trans.* 64 (4) (2016) 525–531.
- [35] R. Grzejda, Impact of nonlinearity of the contact layer between elements joined in a preloaded bolted flange joint on operational forces in the bolts, *Mech. Mech. Eng.* 21 (3) (2017) 541–548.
- [36] W. Zhang, M. Hao, Z. Chang, Y. Wu, P. Tang, H. Chen, Augmentation Plate of a multidimensional cross locking plate versus a locking compression plate for the treatment of femoral shaft nonunion: finite element analysis, *Med. Eng. Phys.* 83 (2020) 106–111, <https://doi.org/10.1016/j.medengphy.2020.05.013>.
- [37] S. Kim, S. Chang, D. Son, Finite element analysis of the effect of bending stiffness and contact condition of composite bone plates with simple rectangular cross-section on the bio-mechanical behaviour of fractured long bones, *Composites Part B-engineering* 42 (2011) 1731–1738.
- [38] A. Jabran, C. Peach, Z. Zou, et al., Parametric design optimisation of proximal humerus plates based on finite element method, *Ann. Biomed. Eng.* 47 (2019) 601–614, <https://doi.org/10.1007/s10439-018-02160-6>.
- [39] D. Jiang, S. Zhan, Q. Wang, M. Ling, H. Hu, W. Jia, Biomechanical comparison of locking plate and cancellous screw techniques in medial malleolar fractures: a finite element analysis, *J. Foot Ankle Surg.* 58 (6) (2019 Nov) 1138–1144, <https://doi.org/10.1053/j.jfas.2018.10.005>.
- [40] L. Le, A. Jabran, C. Peach, L. Ren, Effect of screw thread length on stiffness of proximal humerus locking plate constructs: a finite element study, *Med. Eng. Phys.* 63 (2019 Jan) 79–87, <https://doi.org/10.1016/j.medengphy.2018.12.004>.
- [41] J. Li, M. Wang, J. Zhou, H. Zhang, L. Li, Finite element analysis of different screw constructs in the treatment of unstable femoral neck fractures, *Injury* 51 (4) (2020 Apr) 995–1003, <https://doi.org/10.1016/j.injury.2020.02.075>.
- [42] D. Mischler, S. Babu, G. Osterhoff, C. Pari, J. Fletcher, M. Windolf, B. Geuorguiev, P. Varga, Comparison of optimal screw configurations in two locking plate systems for proximal humerus fixation - a finite element analysis study, *Clin. Biomech.* 78 (2020 Aug) 105097, <https://doi.org/10.1016/j.clinbiomech.2020.105097>. Epub 2020 Jun PMID: 32623297.
- [43] M. Tilton, A.D. Armstrong, H. Wee, M.W. Hast, G. Manogharan, G.S. Lewis, Finite element-predicted effects of screw configuration in proximal humerus fracture fixation, *J. Biomech. Eng.* 142 (8) (2020), <https://doi.org/10.1115/1.4045907>.
- [44] J. Wang, X. Zhang, S. Li, B. Yin, G. Liu, X. Cheng, Y. Zhang, Plating system design determines mechanical environment in long bone mid-shaft fractures: a finite element analysis, *J. Invest. Surg.* 33 (8) (2019) 699–708.
- [45] J. Wang, J.X. Ma, B. Lu, H.H. Bai, Y. Wang, X.L. Ma, Comparative finite element analysis of three implants fixing stable and unstable subtrochanteric femoral fractures: proximal femoral nail antirotation (PFNA), proximal femoral locking plate (PFLP), and reverse less invasive stabilization system (LISS), *Orthop Traumatol Surg Res* 106 (1) (2020) 95–101, <https://doi.org/10.1016/j.otsr.2019.04.027>.
- [46] C. Wang, X. Li, W. Chen, C. Wang, Y. Guo, H. Guo, Three-dimensional finite element analysis of intramedullary nail with different materials in the treatment of intertrochanteric fractures, *Injury* 52 (4) (2021) 705–712, <https://doi.org/10.1016/j.injury.2020.10.102>.
- [47] Y. Wang, J. Wang, S. Tu, S. Li, J. Yi, H. Zhao, H. Qiao, K. Yan, B. Liao, Biomechanical evaluation of an oblique lateral locking plate system for oblique lumbar interbody fusion: a finite element analysis, *World Neurosurg* 160 (2022) e126–e141, <https://doi.org/10.1016/j.wneu.2021.12.105>.
- [48] W. Sheng, A. Ji, R. Fang, G. He, C. Chen, Finite element- and design of experiment-derived optimization of screw configurations and a locking plate for internal fixation system, *Comput. Math. Methods Med.* 21 (2019), <https://doi.org/10.1155/2019/5636528>.